AN INVESTIGATION OF THE NONSTEADY INTERACTION OF A CONDUCTING GAS CLOUD WITH A GIVEN ELECTRICAL CIRCUIT

V. A. Derevyanko, L. A. Zaklyaz'minskii, S. S. Katsnel'son, A. Yu. Kerkis, E. F. Lebedev, N. A. Trynkina, and V. P. Fomichev

Zhurnal Prikladnoi Mekhaniki i Tekhnicheskoi Fiziki, Vol. 9, No. 2, pp. 59-67, 1968

The behavior of a cloud of conducting gas obtained from a coaxial plasma gun is investigated as it passes through a constant magnetic field. The way that this cloud interacts by induction with an electrical circuit coupled to an ohmic resistance is also studied. Paticular attention is paid to the study of the energy characteristics of the interaction (the energy generated in the ohmic resistance, relations between the plasma energy and Joule dissipation) as a function of the geometry and certain parameters of the electrical circuit. The process is analyzed theoretically for small values of the magnetic Reynolds number. Experimental and theoretical results are compared.

1. **The experimental apparatus and the parameters of the working gas (plasma cloud).** The experimental apparatus, a plan of which is given in Fig. 1, consists of a coaxial plasma gun, a radial channel, and a dc electromagnet which creates a magnetic field in the direction of the z-axis. The numerals 1, 2, 3, and 4 denote electrical circuits with inductances L_1, L_2, L_3, and L_4.

When the battery of condensers was discharged, the plasma cloud formed in the gun passed along a tube of heat-resistant glass and into the channel where it expanded radially (in a direction normal to that of the applied magnetic field). All the experiments were carried out with air at an initial pressure of 0.7 mm Hg. The battery capacitance was 600 μF, and the charge voltage was 5 kV. The channel had the following dimensions: a maximum radius of 105 mm, and a minimum radius at the entrance of 25 mm; the channel width was 15 mm at a radius of 25 mm, and subsequently decreased smoothly to 6 mm at the outlet. The constant magnetic-field strength could be varied from 0 to 5 kOe.

Electrical circuit loops for picking up the magnetic field deformation caused by the gas were mounted in the channel walls as were various detectors for measuring gas and electromagnetic field parameters. The electric circuit loops were situated concentrically in planes perpendicular to the z-axis, and as close as possible to the working gas—at a distance of 1 mm from the inner surface of the channel wall. The following were also fitted to the channel wall: probes for measuring strength of the axial magnetic field H; loops to measure the strength of the azimuthal electric field E; solenoids of "open" Rogowski loops (the distant parts of the loop passing through the plasma) for registering the current density j in the plasma, and piezometers. The velocity of radial plasma motion u and the structure of the plasma cloud were studied with an SFR camera. Cloud parameters in the tube before entering the magnetic channel were studied using a piezometer, an SFR camera and an induction device for measuring electrical conductivity [1, 2]. Several plasma clouds pass along the tube depending on the half-periods of the current discharge.

A photograph is presented in Fig. 2a showing the first (u = 24 km/sec), second (u = 16 km/sec) and third plasma formations; the photograph was made with an SFR camera; the motion of the plasma was parallel to that of the image on the film. The reading of the electrical conductivity detector σ is given in Fig. 2b (the time markers occur every 1 μsec, and the maximum signal amplitudes are proportional to the product σu^2). The conductivity σ reaches its maximum value directly behind the luminous front of the leading region of the first plasma formation. Here σ is constant over a length of 60-80 mm with a value of 65-70 $ohm^{-1}\ cm^{-1}$. Further on along the cloud, σ decreases sharply and does not exceed 10 $ohm^{-1}\ cm^{-1}$ in the tail of the first and subsequent plasma formations. Thus, we may suppose that basically only the leading portion of the first cloud interacts with the magnetic field in the radial channel. Its velocity before entering the channel was equal to 24 km/sec.

Pressure measurements made by the piezometer (Fig. 2b; crystal diameter 1 mm, time markers every 1 μsec) show that the cloud is inhomogeneous and the pressure oscillations at the wall of the pipe correspond to the passage of the dark or light regions of the cloud past the detector.

Since the device for measuring electrical conductivity takes an average over some volume, it is insensitive to these inhomogeneities and gives good reproducible readings. The measured cloud parameters differ from those calculated for a one-dimensional shock wave moving with the velocity of the leading edge of the cloud (the calculated electrical conductivity and pressure are σ = 200 $ohm^{-1}\ cm^{-1}$ and p = = 6 atm, while the measured values are 65-70 $ohm^{-1}\ cm^{-1}$ and 4.5 atm).

On entering the magnetic channel, the cloud begins to expand radially. The radial velocity of the leading edge of the plasma attains a value of 12 km/sec at a radius of 50 mm, and remains constant at large radii when there is no magnetic field. This is clear from the

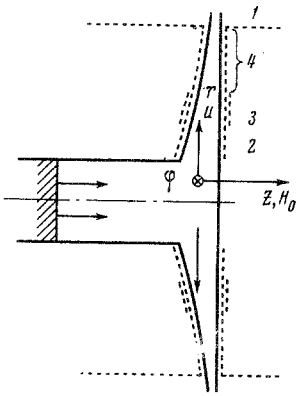

Fig. 1.

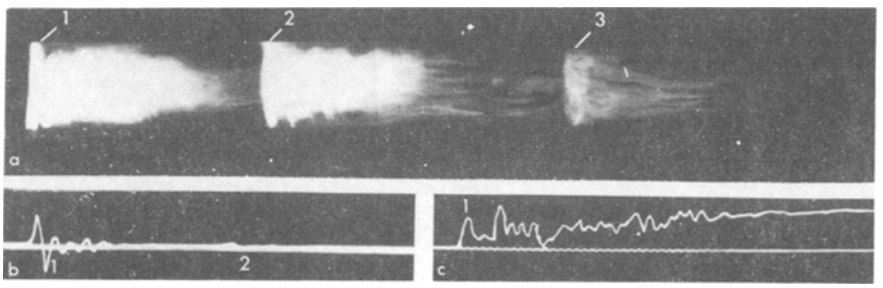

Fig. 2.

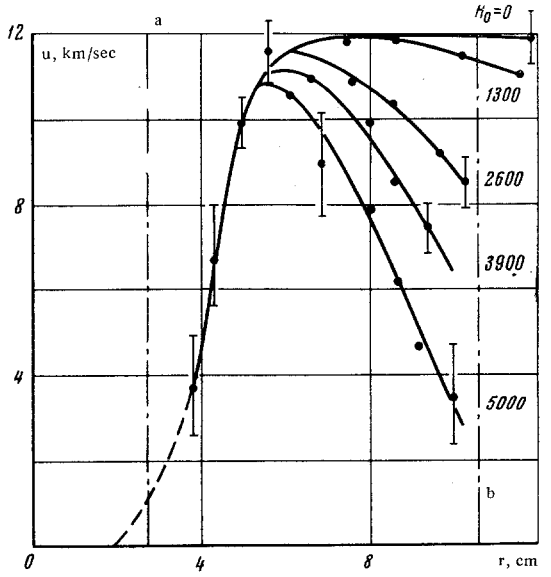

Fig. 3.

curves of Fig. 3 where the velocity of the leading edge (u, km/sec) is given as a function of the radius (r, cm) for various values of the magnetic field H_0, given adjacent to the curves (H_0 was measured at a radius of 65 mm).

The plasma in the channel moved in the form of successive compression waves whose velocity did not significantly differ from the velocity of the leading edge. Figure 4 gives oscillograms of the plasma pressure at the wall of the radial channel corresponding to values of H_0 = 0, 300, 700, and 3000 Oe. The resolution of the detectors was about 1 μsec, the time markers occured at periods of 1 and 5 μsec, and the unit of pressure is 1 atm. The pressure behind the shock wave reflected from the end wall of the channel (r = 0) is equal to p = 80 atm; it remains at this value for several microseconds, and subsequently decreases gradually (Fig. 4a). The plasma pressure at the channel wall attains a value of 1.5 atm for r = 55 mm, and 1 atm for r = 95 mm. The detector, located at a radius r = 55 mm, initially registers a very weak compression wave, and, subsequently, the pressure in the plasma cloud.

It was established by means of the SFR camera and magnetic probes that the plasma pressure is almost axisymmetric in the radial channel. Knowing this, we can investigate the process over the entire volume of the channel using a relatively small number of detectors for making measurements.

The nature of the plasma motion in the channel changes radically when there is a magnetic field. Closed concentric currents arise in the plasma. The ponderomotive forces $\mathbf{f} = c^{-1}\,\mathbf{j} \times \mathbf{H}$ arising as the result of the current density distribution established in the plasma have the greatest effect on the leading edge of the cloud (which is strongly retarded) (Fig. 3).

For a magnetic field strength less than 1000 Oe, the change in the nature of the motion is noticeable only in the regions of large channel radius. The piezometer at a radius of r = 95 mm registers the fusion of two fronts (Fig. 4c). The pressure behind the front becomes equal to the calculated pressure behind a front associated with a plane wave moving at the velocity measured. A similar phenomenon is observed at a radius of r = 55 mm for a field $H_0 \geq 2500$ Oe (Fig. 4d).

Where there is strong retardation of the plasma (up to 3-4 km/sec) the photographic records reveal a weakly luminescent refracted shock wave moving with a velocity close to that of the unretarded plasma (12 km/sec). In this case, the pressure increases smoothly (Fig. 4d) and attains a maximum value of 2.5–3.5 atm. However, the axisymmetric flow in the channel is not disturbed even when there is strong retardation of the gas. Pictures of the plasma motion in the radial channel are given in Fig. 5. They were obtained using the SFR camera; the time between frames is 0.33 μsec; the order of the frames is from top to bottom and from right to left. The pencil of dark lines intersecting the image in this figure is the shadow of the system of magnetic probes registering the symmetry of radial plasma motion. The photographs in Fig. 5 show that the plasma boundary is stable, or, even if a Rayleigh-Taylor instability occurs, it cannot develop sufficiently to disturb the symmetry of flow for $H_0 \leq 4000$ Oe. The zone where current flows in the plasma is on the order of the channel length. The current density attains a value of 3.2 kA/cm^2 for H_0 = 4000 Oe.

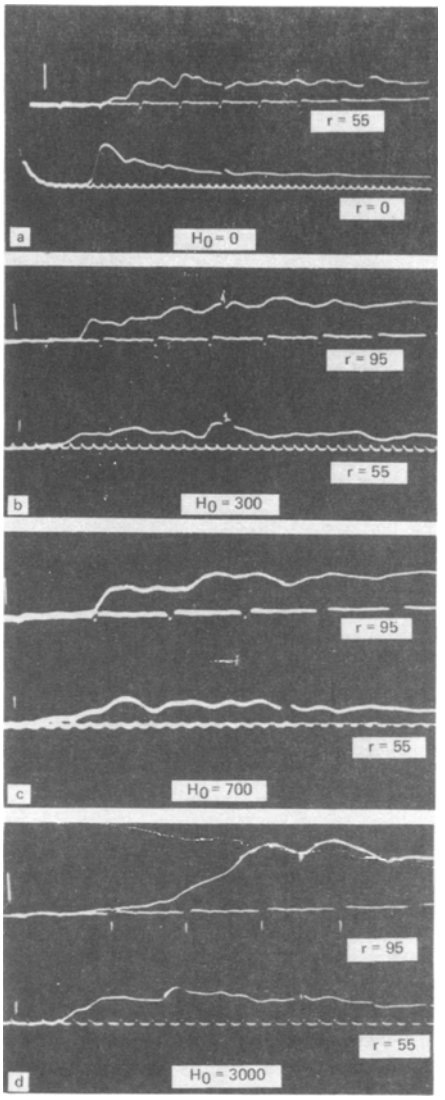

Fig. 4.

The electric-field strength E_j arising from the current in the plasma is an order of magnitude less than the induced field uH/c; for example, E_j = 2 V/cm, and uH/c = 13 V/cm for H_0 = 1300 Oe, while for H_0 = = 4000 Oe, E_j = 5 V/cm, and uH/c = 28 V/cm.

Approximate estimates show that under the prevailing conditions, electrical conductivity of the plasma σ may be taken to be scalar. When σ is calculated from Ohm's law $j = \sigma\,(uH/c - E)$, using the measured values of u, H, E, and j, values of 40–20 ohm^{-1} cm^{-1} are obtained (there is a dependence upon the channel radius; the smaller values refer to larger radii) for $H_0 \leq 1000$ Oe, while σ = 140–80 ohm^{-1} cm^{-1} for H_0 = 4000 Oe. Strong Joule heating of the plasma for large H_0 is also demonstrated. This effect, caused by the currents induced in the plasma, shows up as an increase in plasma luminosity with an increase in the magnetic field strength. A direct calculation of Joule heating over the entire volume of the plasma

$$Q = \int_V \int_t \frac{1}{\sigma} j^2\, dt\, dV$$

give a value of 125 J for H_0 = 4000 Oe.

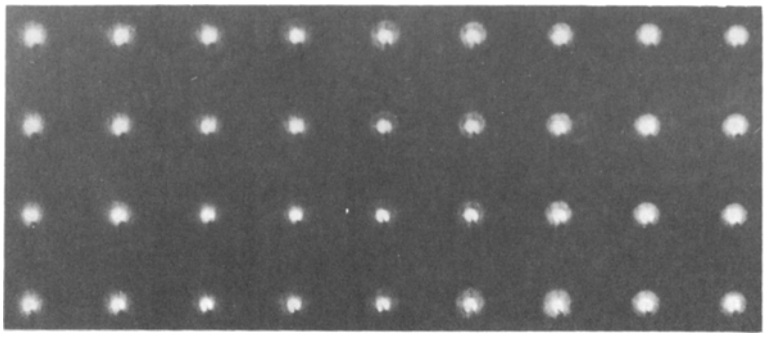

Fig. 5

The magnetic Reynolds number R_m, determined for characteristic dimension equal to the maximum channel radius, varies within the limits 2.5–1.0 depending on the channel radius and the magnetic field strength.

2. **Interaction of the plasma cloud with the electric circuit.** On moving in the radial channel the plasma distorted the magnetic field and produced an emf in the loops of the electric circuit (its presence in the channel wall has already been mentioned above). As a result of this effect, transient currents arising in the circuit led to electric E_k and magnetic H_k fields in the plasma volume.

The effect of these fields on the magnitudes of the total mechanical energy of the plasma A, the Joule heat Q and the useful plasma energy W was investigated as a function of the positioning (geometry) of the circuit loops inductively linked with the plasma, the ohmic resistance of the circuit R, and the strength of the initial magnetic field H_0:

$$W = A - Q = \iint_{V\,t} jE\,dt\,dV$$

$$\left(A = \iint_{V\,t} c^{-1}\,juH\,dt\,dV\right).$$

The electrical quantities A, Q, and W were calculated from the functions j(r, t), E(r, t), u(r, t), and H(r, t) measured in the radial channel. Some components averaged over the channel width were also measured: the azimuthal φ-components of E and j, the r-component of u, and the z-component of H.

Measurements showed that the magnetic field H_k caused by the currents in the electrical circuit was considerably less than the sum of the initial magnetic field H and the field due to the currents in the plasma H_j, i.e.,

$$H_k \leqslant 0.1\ (H_0 + H_j)\ .$$

The electric field E_k of the currents in the circuit was considerably less than the induced field uH/c, but comparable with the field E_j of the currents in the plasma. It follows from this that the presence of the electrical circuit, inductively linked with the plasma and having only an ohmic resistance as a load, has only a small effect on the current density in the plasma, the total plasma energy and the Joule heat under the conditions of our experiment. It also follows that the useful plasma energy is considerably less than the total energy, i.e., $A \approx Q$. The electric field of this circuit does, however, have a marked effect on the useful plasma energy. It is this field which does, in fact, determine the magnitude of the useful energy, since

$$\iint_{V\,t} jE_j\,dt\,dV \ll \iint_{V\,t} jE_k\,dt\,dV\ .$$

That the left-hand side of this expression is nonzero is due to the current induced in the metallic parts of the apparatus. The useful work calculated in this case from the measured values of the current density and electric field and integrated over the whole volume and time of interaction is equal to the energy evolved at the ohmic resistance:

$$W = \iint_{V\,t} jE_k\,dt\,dV \approx \int_t I^2R\,dt\ . \qquad (2.1)$$

We studied four types of windings whose coils were positioned in the following manner.

1. The coils were wound with a radius of 105 mm on the outside of the channel. Its inductance was $L_1 = 400 \cdot 10^{-6}$ H. We denote this type of winding by L_1 (the same as its inductance).

2. The second type of winding is denoted by L_2. The coils (10 coils, 5 on each side) were wound in the channel walls, in spiral form, with a constant pitch of 6 mm, from a radius of 25 mm to a radius of 55 mm. Its inductance was $L_2 = 16 \cdot 10^{-6}$ H.

3. The coils were wound in the form of a dense spiral in two rows with five coils in each row on either side of the channel, situated at radii which varied from 60 to 65 mm. The inductance of the entire winding was $L_{31} = 83 \cdot 10^{-6}$ H. The inductance of the winding L_{32}, which consisted of the two rows closest to the gas, was equal to $L_{32} = 19.8 \cdot 10^{-6}$ H.

4. The coils were wound in the form of a spiral having a constant pitch of 6 mm, from a radius of 65 mm to a radius of 105 mm. Its inductance was $L_4 = 40 \cdot 10^{-6}$ H.

The energy W, J, generated at the ohmic resistance of the electric circuit, is given in Fig. 6a for the windings mentioned above as a function of the magnitude of the resistance. This energy was calculated from formula (2.1) for a magnetic field strength of $H_0 = 1300$ Oe. (The initial magnetic field varied radially from r = 0 to r = 105 mm by a factor of 1.5, and so all indicated values of the field H_0 refer to r = 65 mm. The field H_0 was practically constant over the channel width.)

The marked effect of the winding geometry on the magnitude of the energy generated is clear from Fig. 6a. This effect is governed not only by the mutual induction coefficient between the windings and the currents in the plasma, but also by the magnitude of the current in the circuit, i.e., by the distribution and magnitude of the electric field E_k in the plasma volume due to the current in the circuit.

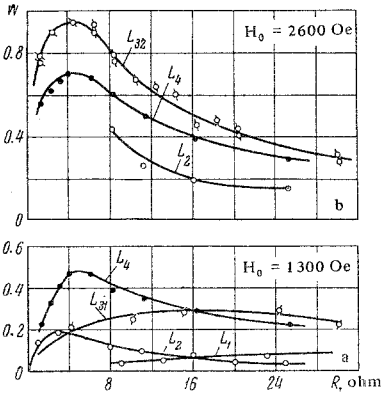

Fig. 6.

Unfortunately, not all the windings are in identically the same condition relative to the nature of the flow. It is clear from Fig. 3 that, in the initial section of the channel, the velocity of radial plasma motion increases rapidly from 0 to 12 km/sec and for $r > 50$ mm, remains constant (if $H_0 = 0$). The winding L_2 was situated in the entrance section of the channel and this region of flow exerted the strongest effect on the inductive interaction between the currents in the plasma and the winding. The field $H_0 = 1300$ Oe has practically no effect on the velocity distribution, so we may assume that the results of Fig. 6a were obtained for unperturbed gas dynamics.

The magnitude of the energy generated at the ohmic resistance is given in Fig. 6b for a field of $H_0 = 2600$ Oe. The gas velocity is markedly diminished for this field, especially at the end of the channel. It is clear, again from Fig. 6b, that the strongest interaction occurs with winding L_3, situated in the region of maximum gas velocity. (For a field of 1300 Oe, the most energy was generated in L_4.) The energy generated is given as a function of magnetic field strength in Fig. 7. For small fields $W \sim H_0^2$; W subsequently attains a maximum and even decreases for large fields.

3. **A theoretical analysis of the process and comparison with experiment.** It is virtually impossible to give a theoretical description of the exceedingly complex nature of the flow in the experimental channel. We therefore take the simplest solution of the equations of gasdynamics as the basis for our theoretical analysis.

The flow may be described approximately by the equations of magnetohydrodynamics taking into account dissipation only in the form of Joule heating, and with an additional equation for the electrical circuit inductively linked with the plasma. If we look for a solution of this system of equations in the form of an expansion in powers of R_m, then, in zeroth approximation, the equations of gasdynamics, Maxwell's equation and the circuit equation are separable. The solution for electromagnetic quantities in first approximation depends upon the gasdynamic quantities in zeroth approximation. One of the solutions of the gasdynamic equations is flow with an entropy wave. Such a flow, with constant velocity, pressure, and arbitrary temperature distribution as functions of the gas particle can exist in a channel of constant cross section. Thus, the gas flow in zeroth approximation may be imagined as follows: there is a cylindrical source of gas at a radius equal to the inner radius of the channel ($r = 25$ mm). Gas flows out of this source with constant velocity and pressure and a temperature which varies periodically in time, and flows in a channel of constant cross section. At a radius of $r = 105$ mm there is a sink which does not perturb the flow.

We have the following components when the axial symmetry of the situation is taken into account (in a cylindrical system of coordinates r, φ, z): the gas velocity has a component only in the direction of the channel radius, i.e., $u_r = u_0 = \text{const}$; the current density **J**, the electric field **E** and the vector potential **A** have the components $J_\varphi(r, z, t)$, $E_\varphi(r, z, t)$, and $A_\varphi(r, z, t)$ only with respect to φ; the magnetic field H has the r and z components $H_r(r, z, t)$ and $H_z(r, z, t)$.

The only electrodynamic quantity in zeroth approximation is the externally applied constant magnetic field in the direction of the z-axis H_0, since, in zeroth approximation, the current in the electric circuit in our case is equal to zero. Thus, in first approximation, the current density in the gas is

$$j = R_m\sigma_0 [E_0 - u_0H_0] = -R_m\sigma_0 . \qquad (3.1)$$

We have the following equation for first-approximation current in the electric circuit:

$$\frac{d}{dt}\sum_n\int_S \mathbf{H}\,d\mathbf{S} + RI_1 = 0 . \qquad (3.2)$$

Here the magnetic flux is summed over the series-connected turns of the circuit.

Equations (3.1) and (3.2) are written in dimensionless form and the characteristic quantities are: l—the channel length, 105 mm; t°—the time; u_0—the velocity; H_0—the magnetic field strength; j°—the current density; E°—the electric field strength; I°—the current in the circuit;

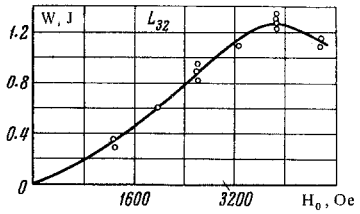

Fig. 7.

σ°—the maximum electrical conductivity of the temperature wave:

$$\left(t^\circ = \frac{l}{u_0},\quad j^\circ = \frac{cH_0}{4\pi l},\quad E^\circ = \frac{u_0H_0}{c},\quad I^\circ = cH_0l\right).$$

Equation (3.2) may be rewritten by introducing the self-inductance of the circuit and the vector potential of the field [3]:

$$\frac{d}{dt}\sum_n\oint_L \mathbf{A}\,dl + L\frac{dI_1}{dt} + RI_1 = 0$$

$$\left(\mathbf{A} = \int_V \frac{\mathbf{j}}{\xi}\,dV,\quad L = \frac{L_0}{l},\quad R = \frac{R_0c^2}{u_0}\right).$$

Here L_0 and R_0 are the actual inductance and resistance of the circuit. Allowing for the fact that there is axial symmetry and, taking Eq. (3.1) into account, we may represent the inductive emf in the form

$$E_{\text{инд}} = -\frac{d}{dt}\sum_n\oint_L \mathbf{A}_1\,d\mathbf{l} = \frac{d}{dt}\sum_n 2\pi r_n\int_V \frac{\sigma_0}{\xi}\cos\psi\,dV ,$$

where ψ is the angle between the vector $d\mathbf{l}$ and the chosen direction φ. Since we do not know the form of the conductivity wave in the experimental apparatus exactly, we specify it in the following general form:

$$\sigma_0 = \sum_i [a_i\cos i\lambda(\tau - t) + b_i\sin i\lambda(\tau - t)],\quad \lambda = \frac{\omega l}{u_0} .$$

Here λ is the dimensionless frequency.

The inductive emf is then equal to

$$E_{\text{инд}} = -\frac{d}{dt}\sum_{i=0}^{\infty}[\beta_i^c(a_i + b_i)\cos i\lambda t + \beta_i^s(a_i + b_i)\sin i\lambda t]$$

$$\left(\beta_i^c = \sum_n 2\pi r_n\int_V \frac{1}{\xi}\cos i\lambda r\cos\psi\,dV,\right.$$

$$\left.\beta_i^s = \sum_n 2\pi r_n\int_V \frac{1}{\xi}\sin i\lambda r\sin\psi\,dV\right).$$

Here ξ is the distance from the point of integration in the gas volume to the circuit loop of radius r_n.

The average power generated in the ohmic resistance over a certain period of time (relative to the quantity $H_0^2u_0l^2$) is then equal to

$$W = R_m^2I_1^2R = R_m^2\frac{1}{L}\sum\frac{\nu i^2\lambda^2}{\nu^2 + i^2\lambda^2}\frac{a_i^2 + b_i^2}{2}(\beta_i^{c^2} + \beta_i^{s^2}) \qquad (3.3)$$

where $\nu = R/L$.

The total energy of the gas per unit time is then (T is the period)

$$A = \int_V \frac{1}{T}\int_t \mathbf{u}(\mathbf{j}\times\mathbf{H})\,dt\,dV = R_m a_0 V + O(R_m^2) .$$

The fraction of energy which is transferred to the external mesh is equal to

$$W = -\int_V \frac{1}{T}\int_t \mathbf{jE}\,dt\,dV =$$

$$= -R_m^2\int_V \frac{1}{T}\int_t \sigma_0\left[\frac{dI_1}{dt}\oint\frac{dl}{\xi} - \frac{\partial}{\partial t}\int_V \frac{\sigma_0}{\xi}\,dV\right]dt\,dV ,$$

where the second term in brackets is the electric field due to current in the gas, and the first is the field due to currents in the circuit. The integral of the second term for this period, over the whole volume, is equal to zero, while that of the first term is $R_m^2I_1^2R$, i.e., the energy

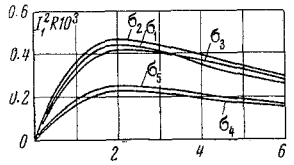

Fig. 8.

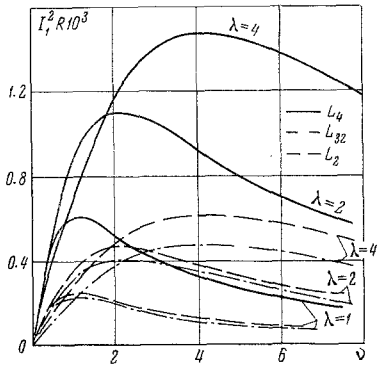

Fig. 9.

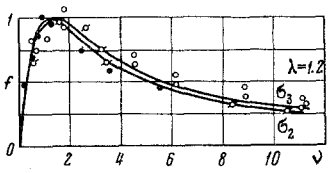

Fig. 10.

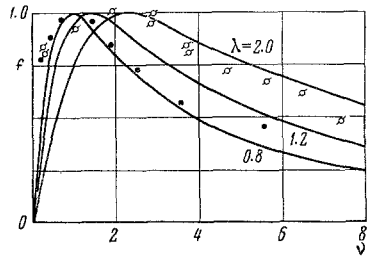

Fig. 11.

transferred to the circuit is determined by the electric field of this circuit only.

The quantity W/R_m^2, calculated from formula (3.3) as a function of ν, λ, and σ_0, and the form of the windings are given in Figs. 8 and 9. The coefficients β_1^c and β_1^k were calculated on an electronic computer. The effect which the form of the conductivity wave exerts on the quantity W is shown in Fig. 8 for $\lambda = 2$ and the winding L_{32}. Here the value of σ was calculated from formulas

$$\sigma_1 = {}^1/_2\,[1 + \cos\lambda\,(r-t)], \quad \sigma_2 = {}^1/_4\,[1+\cos\lambda\,(r-t)]^2$$

$$\sigma_3 = {}^1/_8\,[1+\cos\lambda\,(r-t)]^3, \quad \sigma_4 = \frac{1}{2} - \sum_{m=1}^{\infty}\frac{1}{m\pi}\sin m\lambda\,(r-t)$$

$$\sigma_5 = \frac{1}{3} - \sum_{m=1}^{\infty}\frac{\sin\lambda\,(r-t)}{m\pi} + \sum_{m=1}^{\infty}\frac{\cos\lambda\,(r-t)}{m\pi}\,.$$

A symmetrical wave form turned out to be the most suitable.

The effect of the winding geometry and the wavelength is shown in Fig. 9 where W/R_m^2 is given as a function of ν for various λ, windings L_1, L_3, and L_4 and σ_2. It is clear from the curves of Fig. 9 that the optimum wavelength for all the windings is $\lambda \approx 3$, i.e., roughly twice the channel length. The most suitable of the three windings is L_4, i.e., the winding situated closest to the channel exit.

It also turned out that L_2 was more suitable than L_3, and, in the experiment with $H_0 = 1300$ Oe (Fig. 6a), more energy was generated with L_{31} in the circuit than with L_2. Possibly this is determined by the velocity distribution in the experimental channel (Fig. 3).

We shall attempt to make a qualitative comparison of experimental and theoretical results. In order to eliminate the effect of R_m, we shall take the energy or power relative to its maximum value (for each λ and σ). Thus, Fig. 10 presents the experimental points from Fig. 6a divided by 0.20 J for L_2, by 0.30 J for L_{31}, and by 0.48 J for L_4.

We see that the theoretical curves of σ_2 and σ_3 for $\lambda = 1.2$ are in good agreement with the experimental points. The theoretical curves taken relative to the maximum power, i.e., $f(\nu) = W/W_{max}$, are very much like each other for the various windings when the values of λ and σ are the same. It follows from Fig. 10 that the effective wavelength ($H_0 = 1300$ Oe) is $\lambda = 1$–1.5 for all the windings, i.e., the wavelength is roughly six times the length of the channel. Similar data are given in Fig. 11 for $H_0 = 2600$ Oe. It is clear that the change in the nature of the flow as the field is increased leads to an increase in the deviation of $W(\nu)$ from $\lambda = \text{const}$. for all the windings, which was already noticeable in Fig. 10. We shall now try to make a quantitative comparison of the results. The effective interaction period in the experiment was equal to

$$T = \frac{2\pi}{\omega} = \frac{2\pi l}{\lambda u_0} = \frac{6.28\cdot 10.5}{1.2\cdot 1.2\cdot 10^6} = 46\cdot 10^{-6}\ \text{sec}\,.$$

Using this period we can determine both the average power W^* generated over some period in the optimum ohmic resistance and the value of R_m^* for which the theoretically calculated power is equal to the power which is observed experimentally.

The table given below presents values of W^* for a field $H_0 = 1300$ Oe, as well as the magnetic Reynolds number R_m^* calculated from the ratio of W^* to $H_0^2 u_0 l^2$, and for a type-σ_2 conductivity wave:

	L_2	L_{31}	L_4
$W^*(W)$	$4.4\cdot 10^3$	$6.55\cdot 10^3$	$10.5\cdot 10^3$
$W^*/H_0^2 u_0 l^2$	$1.97\cdot 10^{-1}$	$2.94\cdot 10^{-1}$	$4.5\cdot 10^{-1}$
R_m^*	0.865	1.000	0.800

In the experiment, R_m was equal to 3–6 for small magnetic fields (for a characteristic dimension of $l = 10.5$ cm and effective measured values of $\sigma = 40$–20 ohm^{-1}cm^{-1} and velocity $u_0 = 1.3 \cdot 10^6$ cm/sec).

However, the qualitative correspondence between theoretical and experimental results (Fig. 10) for unperturbed gasdynamics suggests that, in the experimental apparatus, the nature of the plasma interaction with the electric circuit approaches that predicted by theory. This correlation also tends to indicate that the energy in the ohmic resistance is generated by the plasma.

The authors are grateful to G. I. Bagaev, A. P. Morozov, L. N. Puzyrev, and Yu. A. Shadrin for cooperating in the design of the experimental apparatus, and to T. I. Pushkareva and S. P. Mymrina for their assistance in carrying out the experiment and the calculations.

REFERENCES

1. Sh. Ch. Lin, E. Resler, and A. Kantrovits, "Electrical conductivity of highly ionized argon in a shock wave," Voprosy raketnoi tekhniki, vol. 31, no. 1, pp. 11–35, 1956.

2. V. I. Fedulov and G. D. Efremova, "Investigation of a magnetic method for measuring the electrical conductivity of ionized gases," Teplofizika vysokikh temperatur, vol. 4, no. 5, pp. 615–620, 1956.

3. I. E. Tamm, Foundations of Electrical Theory [in Russian], Izd-vo Nauka, 1966.

20 October 1967 Novosibirsk